Surviving the RF Smog: Making Body Area Networks Robust to Cross-Technology Interference

Yantian Hou* Ming Li* Shucheng Yu†
* Department of Computer Science, Utah State University, USA
† Department of Computer Science, University of Arkansas at Little Rock, USA

***Abstract*—Wireless Body Area Networks (BANs) demand for highly robust communication due to the criticality and time-sensitivity of the medical monitoring data. However, as BANs will be widely deployed in densely populated areas, they inevitably face the RF cross-technology interference (CTI) from non-protocol-compliant wireless devices operating in the same spectrum range, which are *persistent, high power, and broadband* in nature. The main challenges to defend such strong CTI come from the scarcity of spectrum resources, the uncertainty of the CTI sources and BAN channel status, and the stringent hardware constraints. Existing methods fail because of their need for extra spectrum resources or advanced hardware. In this paper, we first experimentally characterize the adverse effect on BAN reliability caused by the non-protocol-compliant CTI. Then we propose a CTI-aware joint routing and power control (JRPC) approach to ensure desired reliability goals using minimum energy resources even under strong co-channel CTI. To cope with channel uncertainty, we propose a passive link quality estimation method which exploits prediction. Through extensive experiments and simulations, we show that our proposed protocol can assure the robustness of BAN even when the CTI sources are in very close vicinity, using little overall energy and spectrum resources, and can be easily implemented on commercial-off-the-shelf (COTS) devices.**

I. Introduction

The Wireless Body Area Network (BAN) is envisioned as a key enabling technology for next-generation pervasive healthcare systems. In a BAN, a group of on-body sensors collect and transmit patient's physiological signs using wireless to a controller unit (CU) such as a smartphone. The BAN technology enables more accurate and efficient remote medical diagnosis, and leads to numerous promising applications such as ubiquitous health monitoring and emergency medical response (EMS) [22].

Despite the excitement around the BAN concept, its communication reliability has remained as one of the most challenging technical issues [27]. As BANs are expected to be deployed in densely populated areas including hospitals, homes and emergency theatres, they inevitably face heavy cross-technology interference (CTI) from other RF devices operating in the same increasingly crowded wireless spectrum. For example, the most widely used industrial, scientific and medical (ISM) band (from 2.4GHz to 2.5GHz) is already filled with many CTI sources, including WiFi, Bluetooth devices, and other daily used appliances such as microwave oven, cordless phones, baby monitors, garage doors, etc. Especially, the latter types of devices are less friendly coexisting with BAN transmissions, because of their *persistent, high-power and broadband* nature. For example, a microwave oven usually occupies at least 25MHz in the 2.4G band. In addition, a cordless phone is usually turned on for conversation for several minutes, which persistently emits electromagnetic signal at a transmission power of 1 Watt (or 30dBm), equivalent to 1,000 times of the power limit of medical devices. To ensure high available wireless health monitoring services, the BAN needs to maintain its performance guarantees [27] even under such external and powerful CTI.

One approach to resolve the RF interference is via spectrum licensing, however, the spectrum is becoming increasingly scarcer which makes this harder. The Medical Implant Communications Service (MICS) band spans 402-405 MHz but is dedicated for implanted devices. Although recently, the FCC has allocated additional bandwidth (2360-2400 MHz) for medical BAN services, only those in the 2390-2400 MHz band will be allowed to operate wherever they wish and without coordination of spectrum [6]. As this is adjacent to the ISM band, FCC cautioned that BANs will "need to consider the potential for adverse interaction between their BAN, Wi-Fi and ISM resources" [6]. On the other hand, many existing commercial-off-the-shelf (COTS) medical sensors [27], [31] have adopted one of the wireless technologies under the ISM band. It can be predicted that many BAN applications will still operate in the ISM band. Thus it is imperative to make BANs robust against co-channel CTIs in same band from a technical aspect, instead of waiting for the policy to mandate all the devices to work in a dedicated band.

While there are many existing works on enhancing the co-existence between ZigBee/WiFi/Bluetooth devices, the CTI from *non-protocol-compliant devices* such like electric appliances has received little attention. It is very challenging to mitigate the impact of such CTI in a BAN. All traditional approaches fail due to the strong nature of the interference and stringent device resource constraints of the BAN. For example, spread spectrum cannot deal with high-power CTI, and channel switching is less effective when facing broadband CTI sources, while all the channels are become increasingly saturated. Interference cancellation techniques require advanced hardware as well [9]. On the other hand, due to the complex signal propagation, body movement and posture changes [32], [37], any wireless propagation model is inherently inaccurate, because of the difficulty (if not impossible) to accurately estimate the surrounding environment and body movement. Here, we ask this essential question: is it feasible to deal with this type of commonly encountered powerful CTI in a strictly resource-constrained BAN, without using non-COTS hardware nor significantly modifying the system architecture?

In this paper, we provide a firm answer to this question. Intuitively, our approach finds the most energy-efficient way for all nodes in a BAN to compete with the interference signal (surviving the RF smog), thus effectively enlarges a BAN's "*reliability zone*" subjecting to the maximum sensor power

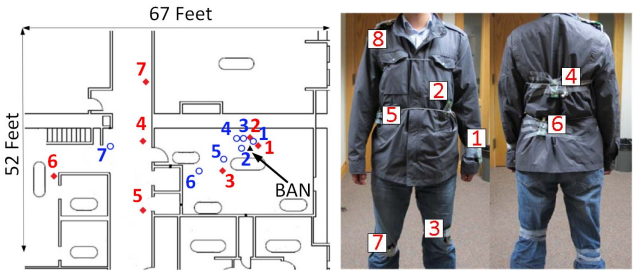

(a) Floor plan and test locations. ♦ - cordless phone, ◯ - microwave oven. (b) Sensor placement on the body.

Fig. 1. Experimental setup

limit. We make four main contributions in this paper:

(1) We carry out an experimental study to characterize the impact of non-protocol-compliant CTI on BAN's performance. We found that a large portion of the links' PDRs can dramatically decrease to 0 when the CTI source is nearby. We also uncover the heterogenous impact of such CTI on BAN links.

(2) This motivates us to propose a CTI-aware optimization framework that simultaneously exploits multi-hop routing and node power control to ensure highly reliable end-to-end data collection in a BAN, while minimizing overall energy consumption. The main novelty is the realistic modeling of channel propagation where packet reception is probabilistic, which is affected by both transmission power, and link qualities under CTI. Because our optimization problem is NP-hard, we propose an effective and efficient heuristic algorithm to solve it.

(3) As accurate link quality estimation under multiple transmit powers is critical for ensuring reliability, we exploit prediction techniques to estimate the uncertain BAN link qualities under external CTI, based only on passive measurements.

(4) We validate the effectiveness of our JRPC protocol through extensive experiments and simulations. Remarkably, we show that JRPC can significantly enlarge the reliability zone of BAN communication under external CTI, even when the interference sources are very close to the human body. JRPC is shown to be very energy-efficient and can be easily implemented on COTS sensor devices.

II. Characterizing the Impact of CTI on a BAN

In this section, we first show through experiments that the high-power and broadband CTI can severely impact the link quality within a BAN. Then we demonstrate that different on-body channels are affected by the interference differently.

A. Experimental Setup

In our experiments we use a Sunbeam SGG5702 microwave oven, and a Uniden EXI4560 2.4 Ghz cordless phone as interference sources[1]. The latter is also not compatible/friendly with wireless networks, as it doesn't switch channel during a call. We use Crossbow Telos RevB sensors with a 802.15.4 compliant transceiver (CC2420) to establish the BAN. We fixed the nodes' channel to Channel 11[2], which overlaps with that of the cordless phone. The transmission rate is set to 250kbps. The

[1]According to [9], the microwave oven mainly occupies the 2.45 - 2.474 GHz spectrum. The cordless phone in our experiment mainly occupies two 5Mhz channels (2.405-2.415 GHz).

[2]We fix the channel because we assume the spectrum is crowded. In reality all other channels may be simultaneously occupied by multiple CTI sources.

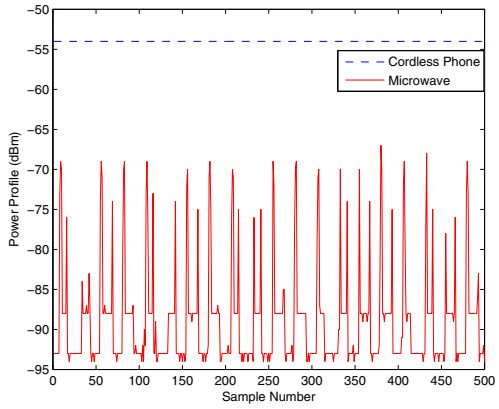

Fig. 2. Microwave and cordless phone interference power levels received by one sensor node on body (sample interval is 0.2ms)

test setup including the locations of the body and interferers are illustrated in Fig. 1(a). For the cordless phone, the handset and base are placed very close (5 cm apart from each other).

For sensor placement (Fig. 1(b)), we put 8 sensor nodes on different places of a human body. Five of them are placed on the front side of body, and two nodes are placed on the back side. Another node is strapped to the left wrist to emulate the CU. In the first experiment, we measure the received interference signal strengths at different nodes. In the second experiment, we measure the packet delivery ratio (PDR) of each link to show the interference's impact on BAN. When experiments start, each node will broadcast a group of 20 probe packets to all the other nodes in turn, using the lowest power level (-25dBm).

B. Impact of Cross-Technology Interference on BAN

We first show the RSS of interference at one node. We measured the interference from cordless phone and microwave oven separately. As is shown in Fig. 2, the RSS from both CTI sources are much stronger compared with background noise (around -93 dBm). For the cordless phone, the signal strength is about -55 dBm and remains constant. For the microwave oven, its power level displays a nearly periodical "ON" and "OFF" pattern over time, which has a roughly 10ms period.

Next we show the impact of CTI on all the 56 links of the BAN. In Fig. 3, we plot the PDR distribution for each scenario with different interference sources and locations. From this figure, we can find that the BAN links are interfered to different extents in different scenarios. For example, nearly 90 percent of links' PDRs are nearly 1 when no interference is presented. However, for the cordless1 scenario, we find that nearly 80 percent of links' PDRs are nearly 0. This phenomenon indicates that the high-power and wide-band cross-technology interference can have severe impacts on BAN's reliability. Besides, there is a correlation between the distance from the BAN to the CTI source and the BAN's reliability - the nearer the CTI source, the PDRs tend to be smaller.

C. Making Use of Heterogeneous Link Qualities

One can also see from Fig. 3 that in each scenario, the links' PDRs show a heterogeneous distribution. This implies that good-quality and bad-quality links simultaneously exist in a

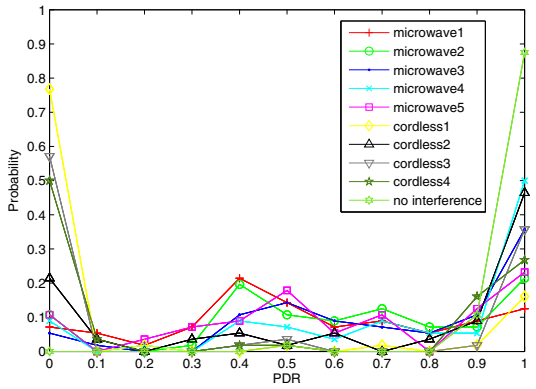

Fig. 3. PDR distribution of all BAN links under various scenarios

from	node 1	node 2	node 3	node 4	node 5	node 6	node 7	node 8
to node 1	/	1	0	0.9	0	1	1	0
to node 6	0.95	0.5	1	1	0	/	1	1

TABLE I
EXAMPLE PDR IN SCENARIO CORDLESS4

BAN under interference. However, a closer look at the cordless4 scenario reveals that many direct links from sensor nodes to CU are severely impacted. The interference causes three links' PDRs to drop dramatically to 0 - links $3 \rightarrow 1$, $5 \rightarrow 1$ and $8 \rightarrow 1$. This is due to the larger body shadowing and longer distance of those direct links, which causes a packet's RSS to fall below that of the interference's. On the contrary, some other on-body links have better qualities due to their smaller path losses (nodes can be closer to each other and in line-of-sight). Basically, according to the PDR-SNR relationship of sensor devices [36], a packet's RSS needs to overpower that of interference's to make the packet delivered.

To this end, a straightforward method is to enhance the transmission power of nodes' direct links to CU. However, there are two issues with this approach: (1) Even when those direct links use the maximum possible power (0dBm), there still exists a significant region where BAN communication is disrupted, as we will show in Sec. V. This is mainly due to the very high-power nature of interference. (2) It may not be the most energy-efficient way. Thus, to enlarge the "*reliability zone*" of a BAN under interference and minimize energy consumption, we are motivated to simultaneously exploit the remaining good-quality on-body links (for multi-hop transmission) and power control. In the same scenario (Table 1), the PDR from node 3 to node 1 is 0, the one from node 3 to node 6 ($= 1$) and the one from node 6 to node 1 ($= 1$) are still high. Suppose node 3 needs to use 0dBm (assume node power: 20mW) to achieve a PDR of 1 while -25dBm requires 8mW. Therefore, we can find a path $3 \rightarrow 6 \rightarrow 1$ with high E2E PDR ($= 1$) with power consumption of $8 + 8 = 16mW$ to transmit a packet for node 3 to 1. In contrast, if we use $3 \rightarrow 1$, this will be $20mW$.

III. PROBLEM FORMULATION

In this section, we first present the models and assumptions, and then formulate the JRPC problem. After that we introduce the main challenges in solving this problem.

A. Models and Assumptions

1) Network and Traffic Model: In this paper we consider the routine convergecast data collection communication in a BAN, where each on-body sensor generates and sends a data packet to the CU periodically at constant rate R_s (packets/second). We model the BAN topology as a directed graph $G(V, E)$ and $N = \mid V \mid$, where V is the set of all nodes and E is the set of all links. For each link (i, j) we use $\lambda_{i,j}$ to denote its PDR, which is the probability that a packet sent by i can be directly received by j. Meanwhile, for each node i, we use λ_i to denote the probability that a packet sent by i can be received by the CU (possibly through multi-hop), which is called E2E PDR.

At the link layer, we turned off the CSMA mechanism and adopted a TDMA MAC mechanism which yields bounded delay. For periodical data collection applications, it has been shown that TDMA is better [4]. Time is divided into slots with equal length T - the time needed to transmit one data packet. A "source cycle" $T_S = \frac{1}{R_s \cdot T}$ refers to the number of slots between two consecutive packet generation events. We use "data cycle" T_D to represent the number of slots needed to transmit all source packets in one source cycle to the CU, and packet retransmission is not considered. Note that, at each time slot, only one link can transmit to avoid packet collision, because the nodes in a BAN are usually considered to be in each other's radio range. Obviously, $T_D \leq T_S$ is necessary to avoid any source congestion.

2) Interference Model: It is difficult to model the CTI exactly, as in practice the number and types of them are uncertain. Instead, we will model the impact of the CTI on link quality later, by only assuming that in a short time period T_{big} the RSS of the aggregated CTI $\mathcal{I}$ sensed by a node is a stationary random process, which is a minimal assumption. Though we focus on non-protocol-compliant CTI, this model is applicable to general CTI.

3) Energy Model: We consider each sensor node to have L different transmit power levels $\{P_1, P_2, ..., P_L\}$ (for a TelosB sensor $L = 8$). We denote the transmit power on each link as $l_{i,j}$. Assuming the circuit power P_{cir} is a constant, then we can obtain the power spent by the transmiter/receiver on each link:

$$P_{tx}(l_{i,j}) = P_{cir} + P_A(l_{i,j}) \quad (1)$$

$$P_{rx}(l_{i,j}) = P_{cir} \quad (2)$$

where $P_A(l_{i,j})$ is the additional circuit power for $l_{i,j}$. Note that this model has also been adopted by previous work [34].

B. Design Objectives

To cope with cross-technology interference in BAN, we aim at ensuring a certain reliability requirement for each sensor node communicating with the CU, while using a minimum overall energy consumption.

(1) *Reliability requirement*: For each node i in a BAN, we require its E2E PDR to the CU λ_i should not be less than a predefined threshold $\lambda_{th} \in [0, 1]$. Delay is another important concern in some BAN applications; so our design also keeps reducing delay in mind.

(2) *Energy consumption minimization*: The overall energy consumption accounts for the transmission and reception of all the packets by all nodes. It is proportional to that in one source cycle length, as a feasible source rate requires that $T_D \leq T_S$.

Although we do not explicitly ensure a throughput goal (various nodes may have different throughput requirements),

it is closely related to the E2E PDR and delay. Using a back-of-the-envelope calculation, we show the feasible rates in our scheme suffice for most BAN applications. In reality, the data rate of CC2420 is 250 kbps. Suppose our algorithm yields $T_D = 15$ slots for a BAN with 8 nodes, then each node has a data rate of $250/15 = 16.6$ kbps. The throughput would be relatively smaller if considering the overhead (header, processing delay). However, this rate should be sufficient for most of the BAN applications, e.g, heart/pulse rate and body temperature whose minimum data generating rates are $60Hz$, or the more demanding EEG applications requiring $1KHz$ sampling rate [27].

C. Surviving Interference through Joint Routing and Power Control (JRPC)

We give the formulation of the JRPC problem in Eqs. (3) - (9). Our goal is to find a convergecast routing tree $G' = (V, E')$, and link power level assignments $l_{i,j}$ satisfying the formulation.

$$\text{minimize} \quad \sum_{(i,j)\in E'} \frac{P_{tx}(l_{i,j}) r_{i,j} T}{R_s} + \sum_{(j,i)\in E'} \frac{P_{rx}(l_{j,i}) r_{j,i} T}{R_s} \tag{3}$$

$$\text{subject to} \quad \lambda_i = \prod_{(j,k)\in \text{Path}(i,1)} \lambda_{j,k} \geq \lambda_{th}, \forall i \in V \setminus 1 \tag{4}$$

$$\lambda_{i,j} = g_{i,j}(l_{i,j}, \mathcal{I}), \forall (i,j) \in E \tag{5}$$

$$\sum_{(i,j)\in E'} \frac{r_{i,j}}{R_s} \leq \frac{1}{R_s \cdot T} \tag{6}$$

$$\sum_{(i,j)\in E'} r_{i,j} - \sum_{(k,i)\in E'} r_{k,i} = \begin{cases} R_s, \forall i \in V \setminus 1 \\ -(N-1)R_s, i = 1 \end{cases} \tag{7}$$

$$E' \subseteq E, \ (V, E') \text{ is a tree} \tag{8}$$

$$l_{i,j} \in \{P_1, P_2, ..., P_L\}, \forall (i,j) \in E' \tag{9}$$

In the above, Eq. (3) is the overall energy consumption in one source cycle. Eq. (4) is the E2E PDR constraint, where λ_i is the product of all the links' PDRs $\lambda_{i,j}$ on the path from i to CU. In Eq. (5), $g_{i,j}(\cdot)$ is the mapping from the transmit power level to link PDR for each link, given the external CTI. This will be derived at the beginning of each big slot by our link PDR estimation algorithm. Eq. (6) refers to the condition $T_D \leq T_S$ of feasible source rate, where $r_{i,j}$ is the traffic rate on each link (packets/second). Eq. (7) is the network flow conservation condition; Eq. (8) and Eq. (9) are constraints on the output routing tree and link power levels, respectively.

The objective function (3) and constraints (4) and (5) are all non-linear (P_{tx} is a non-linear function of $l_{i,j}$ [39]). Therefore the above is a *non-linear integer programming* (NLIP) problem, which is known as NP-hard.

D. Main Challenges

There are two main challenges in solving the above problem. First, how to obtain the link PDR $\lambda_{i,j}$ under any transmit power and given the uncertain CTI and BAN channel status (mapping $g_{i,j}(\cdot)$)? To do this we need to know each link's SINR under various transmit powers. However, it is inaccurate to apply channel propagation models to estimate the received packet RSS due to the channel dynamics. Traditionally link PDR has been estimated by actively sending probe packets [14], [19], [20]. However, to obtain the PDR estimation under different transmission powers, it is impossible to send probe packets using every power level.

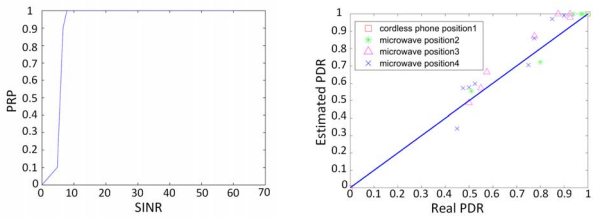

(a) The measured PRP-SINR relation for sensors. (b) Accuracy of link PDR estimation under various power levels.

Fig. 4. Link PDR estimation under CTI.

Second, it is difficult to approximate the NLIP's optimal solution in polynomial time as it is *non-convex and non-separable*. Also, the mapping $g_{i,j}(\cdot)$ in Eq. (5) is given as input in practice, which does not have a mathematical expression. Even if an approximation algorithm is found, it can be too computationally demanding to be used in COTS sensors.

IV. Our Solution: the JRPC Protocol

In this section, we first introduce our basic idea to solve the JRPC problem. Then we present our protocol, including its key components and some analytical results, along with a complexity analysis.

A. Protocol Overview

To tackle the first challenge, we exploit prediction to estimate the links' PDRs under various power levels, which is taken as input to our optimization problem. To solve the second one, we propose an effective and efficient heuristic algorithm (JRPC).

Our protocol consists of two phases. Time is divided into big slots of duration T_{big} consisting of multiple source cycles T_S. First, at the end of each big slot, every BAN node passively measures their incoming link's PDR in the current slot based on the received data packets and sensed interference signals, and estimate the mappings $g_{i,j}$ from $l_{i,j,k}$ to their corresponding $\lambda_{i,j,k}$ at all transmit power levels $k \in [1, ..., L]$. These information are sent to the CU, who predicts the links' PDRs $\lambda_{i,j}$ for the next big slot under all power levels.

In the second phase, using the $g_{i,j}$ as input, the JRPC algorithm is ran to establish the routing tree and assign node power levels, while minimize the energy consumption and guarantee the reliability requirement. Our JRPC algorithm is a greedy algorithm in nature. Basically, we first use a variant of Dijkstra's algorithm to build a maximum E2E PDR tree to maximize the reliability of the BAN in the presence of external CTI. Then we decrease the transmission power levels of all the nodes as much as possible while satisfying the E2E PDR constraints. In this way, our algorithm can always guarantee the E2E PDR requirement whenever the optimal solution does. To evaluate the effectiveness of JRPC, we will compare it with a lower bound of the optimal solution in Sec. V.

B. Link PDR Estimation and Prediction under CTI

To assure reliability under external CTI in our optimization framework, a key issue is to accurately estimate the link

qualities with minimum overhead. The essential question is, for every link (i, j), which transmission power level yields the desired PDR? Previous link power control approaches [35] did not consider CTI, which makes it easy to determine the desired transmit power as the relation between PDR and SNR can be measured in advance. However, under external CTI there is no such simple fixed relation. New modeling techniques must be developed. Thus our solution estimates the dynamic link PDR-transmit power relation *on the fly*. First, at the end of each big slot, nodes will compute/estimate the the PDR of all incoming links under various power levels based on passive measurements on data packets and CTI. Second, we will exploit prediction to estimate the transmit power-link PDR mappings of next big slot, based on previous records.

1) Estimating Link PDR - Transmit Power Relation: As we know, the probability of successful packet reception is a function of that packet's SINR (signal-to-interference-and-noise-ratio). However, under CTI, the SINR is dynamic (due to the uncertainty of CTI sources and the channel fading). Thus, link PDR estimation bogs down to compute the packet SINR distribution, and map that to a PDR.

First, we determine the relationship of PRP (Packet Receiving Probability for single packet) w.r.t. SINR: $PRP(\gamma_{i,j})$ where $\gamma_{i,j}$ is the SINR. For sensors, the transition phase from 0 PRP to 1 is usually small, which is close to a step function [36]. Our experiments also verify this result (Fig. 4(a)). Theoretically, under interference signal $\mathcal{I}$ and a fixed transmit power, the link PDR is a mean value:

$$\lambda_{i,j} = \int PRP(\gamma_{i,j}) h(\gamma_{i,j}) \mathrm{d}\gamma_{i,j}, \tag{10}$$

where $h(\gamma_{i,j})$ is the distribution of $\gamma_{i,j}$. The difficulty here is how to accurately compute $\lambda_{i,j}$ efficiently in reality because it is non-trivial to derive $h(\gamma_{i,j})$. Thus we approximate $\lambda_{i,j}$ by exploiting the property of stationary random process - the ensemble mean equals to the temporal mean. Assuming the beginning of a packet distributes randomly over time and the packet RSS $RSS_{pkt,k}$ remains constant, based on a sequence of M consecutive interference RSS samples, we obtain an estimation of PDR when transmit power is P_k:

$$\lambda_{i,j,k} = \frac{1}{M} \sum_{l=1}^{M} PRP(\gamma_{i,j,k}(l)), \tag{11}$$

where $\gamma_{i,j,k}(l) = \min\{RSS_{pkt,k} - RSS_{\mathcal{I}(l)}, \cdots, RSS_{pkt,k} - RSS_{\mathcal{I}(l+\Delta)}\}$. This is because of one packet transmission duration spans several (Δ) interference RSS samples, while whenever one part of the packet is corrupted the whole packet cannot be received correctly (error correction code is not implemented in 802.15.4). As the channel fading is usually not significant in a big slot, we set $RSS_{pkt,k}$ as the average packet RSS to average out the effect of fading. In addition, since the wireless channel can be regarded as a linear system, for any transmit power level P_k (dBm) we have:

$$RSS_{pkt,k} = RSS_{pkt,0} + P_k - P_0, \tag{12}$$

where P_0 is the transmit power in the current big slot. Combining the above, we can derive the mapping $g_{i,j} : l_{i,j,k} \rightarrow \lambda_{i,j,k}$, merely using passive measurements under one power level.

Algorithm 1 Building maximum E2E PDR tree

input: graph $G(V, E)$, links' PDRs $\{\lambda_{i,j,L}\}_{(i,j)\in E}$
output: maximum E2E PDR tree topology T

```
Insert CU node 1 into tree T; λ_1 ← 1.
Put all other nodes into set S
while S ≠ ∅ do
    Select the node d with maximum λ_d from T.
    if there are ties among any set of nodes then
        Select the node that brings the minimum ΔE.
    end if
    Insert d into T, delete d from S. Update λ_j ← max_{∀i∈T}{λ_i·λ_{i,j,L}}
  for all j ∉ T.
end while
```

We design an experiment to validate the effectiveness of our link PDR estimation algorithm. We put two nodes on different locations of the body, and let one of them transmit 40 probe packets to the other for 8 rounds, each round using a different power (from -25dBm to 0dBm). We record the actual PDRs in each round, but only the average packet RSS and interference samples in the first round (using minimum power -25dBm). Then we run the estimation algorithm to compare the estimated PDRs with real ones for the other 7 rounds. We use $\Delta = 8$ for a 1.6ms long packet, since the interference sample interval is $0.2ms$; also $M = 100$. Results are shown in Fig. 4(b). It can be seen that the estimated and real PDR match well.

2) Predicting links' PDRs under Various Power Levels: For each of the past T_{big} period, each node j obtains a list of PDR estimations under all power levels: $\{\lambda_{i,j,k}\}_{i\neq j, 1\leq k\leq L}$. Based on these historical data, j can predict the link quality under every power level for the next big slot using **autoregression** (AR). The AR model is a tool for predicting a time series of data [25]. Formally $AR(p)$ is defined as: $z_k = c + \sum_{i=1}^{p} \phi_i z_{k-i} + \epsilon_k$, where c is a constant, ϕ_i is AR coefficient, and ϵ_k the zero-mean Gaussian white noise error. This model can be updated continuously as new samples arrive to ensure accuracy. A concrete model can be found in [16], [18]. Intuitively, the AR exploits the correlation inside the time series; it fits our problem as the CTI is persistent in nature. Our method has low overhead and does not need special probing packets.

C. Solving the JRPC Problem

To solve our JRPC problem, we first observe that when the links' PDRs are binary variables, there is a simple polynomial time optimal algorithm. Then we explore the general case and propose an effective heuristic algorithm.

1) Binary Link PDR Model: When the RSS from CTI remains a constant over time (such like a cordless phone), due to the step-function like PRP-SINR relationship, the links' PDRs are in fact close to binary 0-1 values. Thus, it is interesting to discuss this representative special case, which is of theoretical and independent interest.

In this case, due to the monotonicity of the function between link PDR and power level, we can find the minimum power level $P_{i,j,min} = P_{tx}(l_{i,j,min}) + P_{rx}$ of each link that guarantees $\lambda_{i,j} = 1$. If we set $P_{i,j,min}$ as the weight of each link, the Dijkstra's algorithm can be adopted directly to find the "shortest" path from each node to the sink. Since the summation of all the paths' energy consumption equals to our objective function Eq. (3), the total energy consumption in a TDMA cycle is minimum.

2) Continuous Link PDR Model: Under the general case where the links' PDRs are continuous, our proposed JRPC algorithm consists of two steps.

Construction of Maximum E2E PDR Tree Our primary goal is to ensure BAN's reliability under the presence of interference. Therefore, we first build a maximum reliability tree to guarantee that we can find a feasible solution to our JRPC problem whenever it exists. The idea is to set the power level for each node at the maximum, because the E2E PDR for each node is a non-decreasing function of any link's transmit power. Then we use a variant of Dijkstra's algorithm, where the difference with the standard Dijkstra's algorithm is that, the links' weights are their corresponding PDRs, and the "shortest path" metric is replaced by the minimum E2E PDR, which is computed by multiplying all the links' PDRs on each path and take the maximum. Specifically, in each step of the algorithm, we always insert the node i which has the maximum E2E PDR λ_i into the tree. To resolve ties, we insert the node which brings the minimum additional energy consumption (ΔE, which equals the tx/rx power sum of all the links from it to the root) to the existing tree. By doing so, in the resulting tree every node's E2E PDR achieves the maximum. The algorithm is described in Alg. 1.

Decreasing Node Power Levels In this step we decrease the transmit power level of each node based on the derived max-E2E PDR tree. Our objective is to minimize the overall energy consumption while satisfying the E2E PDR requirement $\lambda_i \geq \lambda_{th}$ for all nodes. The essential question is which order should we follow to decrease nodes' transmit powers.

Therefore, we propose a greedy strategy, in which the transmit powers of the nodes at higher levels of the tree are decreased first. The intuition is, the higher a node's level, the more transmitting opportunity (traffic load) it has, thus decreasing its power level first is more effective for the overall energy reduction. However, care should be taken as changing one node i's transmit power may affect all the nodes lower than i in the tree. Thus, for each node i from top to the bottom level (except the CU), we continue to decrease its transmit power level until any node j in i's subtree's E2E PDR $\lambda_i < \lambda_{th}$ (including i itself). This algorithm is depicted in Alg. 2.

Protocol Summary In our protocol, in each big slot, every on-body node j first measures and records the RSSes of the received *data packets* from each node $i \neq j$ sent using some power P_0. After all nodes finish transmitting, each node will record M consecutive samples of the CTI's RSS. Then each j will estimate $\lambda_{i,j,k}, \forall i \neq j$ under all other power levels $P_k \neq P_0$ using Eqs. (11) and (12), and obtains the following list of links' PDRs under each transmit power level: $\{\lambda_{i,j,k}\}_{k\in[1,\ldots,L]}, \forall i \neq j$. Next, each node sends its list to the CU in the end of the current big slot using the current power and routing scheme. Based on the historical data, the CU first predicts the links' PDRs for the next big slot and obtains $\{\widehat{\lambda}_{i,j,k}\}_{k\in[1,\ldots,L]}, \forall i \neq j$, runs our JRPC algorithm using this input, and then broadcasts the new power and routing assignments to all nodes: $\{i, l_i, n_i\}_{i\in V}$, where l_i and n_i are the power level assignment and the next-hop node of i, respectively.

Algorithm 2 Decreasing Nodes' Transmit Powers

input: tree T, links' PDRs $\{\lambda_{i,j,k}\}_{(i,j)\in E, 1\leq k\leq L}$
output: transmit power levels $P_i, \forall i \in T\backslash 1$

1: Sort all nodes in $T\backslash 1$ in the order of their tree level (top to bottom).
2: **for** all nodes i in the sorted order **do**
$P_i \leftarrow$ the minimum power level s.t. $\lambda_k \geq \lambda_{th}, \forall k \in T$ with level lower than i, include i itself.
3: **end for**

D. Algorithm Analysis

1) Algorithm Effectiveness: Usually the optimality of a heuristic algorithm for an NP-hard problem is evaluated by an approximation ratio expressed in asymptotic notation. However, such an approximation ratio is often not tight enough to bound the algorithm's performance [11], which may not be practical. Thus, we propose a concrete lower-bound to the optimal solution of our JRPC problem, and will compare our heuristic algorithm (an upper bound itself) with it in Sec. V.

A lower bound for the optimal solution. Our basic idea is to relax the node E2E PDR constraints in the original JRPC problem. Instead of requiring $\lambda_i \geq \lambda_{th}, \forall i \in V$, we will find the minimum energy convergecast tree $G'' = (V, E'')$ s.t. $\lambda_{i,j} \geq \lambda_{th}, \forall (i,j) \in E'$ (denoted as Q'). To do so we first find the minimum power level $P_{i,j,min}$ for each link $(i,j) \in E$ s.t. $\lambda_{i,j} \geq \lambda_{th}$. Then we find a shortest path tree (SPT) using $P_{i,j,min}$ as each link's weight, which yields the optimal solution to the relaxed problem Q': $\{P'', G''\}$, with minimum energy consumption $E_{P'',G''}$ (P'': node powers).

Proposition 4.1: The energy consumption $E_{P'',G''}$ is a lower bound of the optimal solution to original JRPC problem.

Proof: In the optimal solution $\{P, G' = (V, E')\}$ to the original JRPC problem, we have $\forall (i,j) \in E'$ $\lambda_{i,j} \geq \lambda_{th}$ (Otherwise $\exists i \in V, \lambda_i < \lambda_{th}$ because $\forall i \in V, \lambda_i = \prod_{(j,k)\in \text{Path}(i,1)} \lambda_{j,k} \geq \lambda_{th}$). Because of the monotonicity of the link PDR - transmit power relation, based on $\{P, G'\}$, we can derive another solution $\{P', G'\}$ by decreasing the power level of each node as much as possible s.t. $\lambda_{i,j} \geq \lambda_{th}, \forall (i,j) \in E'$. This is a feasible solution for the problem Q' (may not be optimal). While our lower bound solution is an optimal one for Q', we have $E_{P'',G''} \leq E_{P',G'} \leq E_{P,G'}$, thus proven. ■

2) Complexity Analysis: The complexity of step 1 in our heuristic algorithm is the same with the Dijkstra's algorithm, which runs in $O((N+m)\log n)$ time in average and $O(N^2 \log N)$ in the worst case ($N =\mid V \mid, m =\mid E \mid$). In step 2, we decrease every node's power level from the top to bottom. For the d-th node in the ordered set, the lower-level nodes in its subtree should not be more than $N-1-d$ (except the root), thus we need to check $N-1-d$ nodes' E2E PDRs at most. For the whole tree, in the worst case we need to compute node E2E PDRs $O(N^2)$ times, as there are $N-1$ nodes. For each node, we have to check for all L power levels at most. As L is a constant, the complexity for this step is still $O(N^2)$.

V. Performance Evaluation

We use both experiment and simulation to validate the performance of our JRPC protocol. First, we implemented our link quality measurement, estimation and prediction algorithms on real Crossbow Telos RevB sensor motes. Based on this we will validate the accuracy of PDR prediction under CTI, using various transmit powers for a single link. This serves as

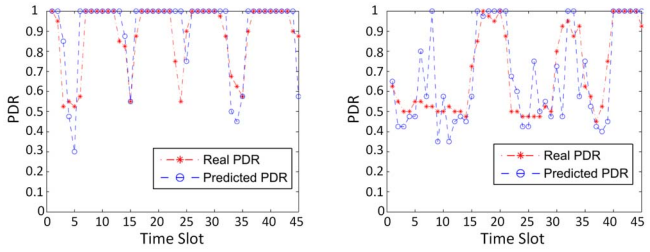

(a) Scenario 1 (b) Scenario 2

Fig. 5. Comparison between predicted PDR and real PDR

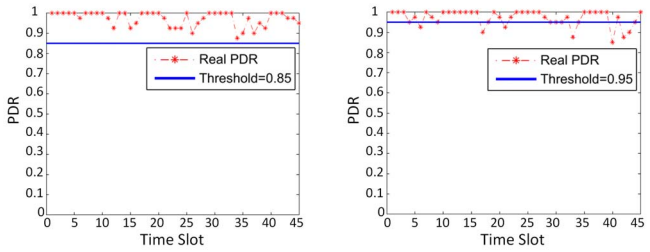

(a) $\lambda_{th} = 0.85$ (b) $\lambda_{th} = 0.95$

Fig. 6. Actual Link PDR under predicted transmit power level.

a primitive operation in each big slot in our protocol. Second, we attach 8 sensors to a human body to emulate the BAN (Fig. 1(b)), from which the {power level, link PDR} pairs for every link in each big slot are obtained. Our JRPC protocol is implemented and simulated on a workstation with Matlab, which uses real inputs from our experiments.

For parameter settings, we set each big slot to contain 40 TDMA cycles, and each TDMA cycle includes S TDMA slots. S is not fixed; it equals to the number of TDMA slots derived from the JRPC algorithm output. Typically S is smaller than 15. We use 250kbps rate and each TDMA slot is 2ms. In each slot a 29-byte packet is transmitted. Based on these parameters, the overall duration of each big slot is smaller than 1.2s. At the end of each big slot, $M = 100$ interference samples are sensed, which is large enough to get whole information of CTI features. Each sample only takes about 0.2 ms, therefore the interference sampling phase is very fast.

A. Accuracy of Link Quality Prediction under CTI

We designed two experiments to validate the effectiveness of our link quality prediction method and the link PDR - transmit power relation estimation. We test using single-link scenarios for simplicity of implementation and analysis. However, the results are sufficient to show that the prediction algorithm can be used in real BANs, as our single-link scenarios take both the channel fading and the dynamics of CTI into account.

In the first experiment, we test the accuracy under a single transmit power (the minimum level, which is the worst case for measurement). We implement the autoregressive algorithm in [16] using an order $p = 2$. The transmitter and receiver are placed on the right knee and left wrist, respectively. To emulate reality in a BAN, the former periodically sends 40 data packets (29 byte payload) with 30ms interval. We use a microwave oven as the CTI source, which is $0.5m - 1.5m$ from the body. In scenario 1, the person sits in a chair. The microwave oven is periodically turned on and off every 10 seconds. In scenario 2, the person periodically walks towards and backwards the microwave oven every 10 seconds while the latter is turned on all the time. The real PDR and predicted PDR are recorded and compared in Fig. 5. From Fig. 5, one can see that our approach can accurately predict the PDR.

The second experiment simultaneously evaluates the effectiveness of link PDR - transmit power estimation and prediction via power control. The person sits in the chair while the microwave is turned on and off. In each big slot, the receiver predicts the link PDR under each power level for the next big slot based on the estimated {power level, PDR} tuples in the past, and it chooses the minimum power level satisfying the PDR threshold and informs the transmitter to use this level in the next big slot. We collect the real PDR sequence to see whether the predicted minimum power level can guarantee the desired PDR on a single link. We set two link PDR thresholds: 0.85 and 0.95. From Fig. 6, one can see that the predicted power level can guarantee link PDR for most of the time. The above results imply that, as long as our JRPC algorithm outputs a feasible link power assignment and routing scheme that satisfies the E2E PDR constraint based on the input transmit power - link PDR relation predicted in each big slot, our protocol can actually ensure the desired E2E PDR for each node in reality.

B. Robustness and Effectiveness of JRPC

We now evaluate the robustness and effectiveness of our JRPC algorithm. Our experiment scenarios include two CTI sources (cordless phone and microwave oven) placed at different locations. Using the collected link qualities as input, we compare the overall energy consumption output by our JRPC algorithm, the lower bound, and a simple star topology using the same single-link power control method as ours.

Figs. 7 and 8 show the energy consumption in one TDMA cycle under the presence of CTI from the cordless phone and microwave oven, respectively. The locations are sorted by increasing distance to the body (see Fig. 1(a) for floor plan), so the CTI is largest in location 1 and smallest in location 7. In Fig. 7, the star topology based power control fails to guarantee the E2E PDR requirement when the cordless phone is at locations 1, 2, and 3, even with the highest transmit power level. *In contrast, remarkably, our JRPC algorithm can always guarantee the E2E PDR (up to 0.98) in the presence of the strong CTI, even when the cordless phone is closest to the body (held beside the head and making a phone call).* This is the same case with microwave oven CTI in Fig. 8. Note that, in our protocol the control packets are treated the same way as data packets, thus their reliability is ensured as well.

Meanwhile, the results also show that our algorithm is very energy-efficient by comparing with the lower bound. The lower bound is either equal to or smaller than the optimal solution. In most scenarios for cordless phone, our algorithm achieves the same energy consumption as the lower bound (as it is close to the 0-1 link PDR case). Only in a few scenarios, such as positions 1 and 2 for microwave oven, the energy consumption is a little higher than the lower bound. This indicates the effectiveness of our heuristic algorithm.

In addition, our algorithm yields low end-to-end delay for each source packet. As we can see from Tables. II and III, assuming TDMA slot is $T = 2ms$, the end-to-end delay values are very small even with the strictest E2E PDR requirement

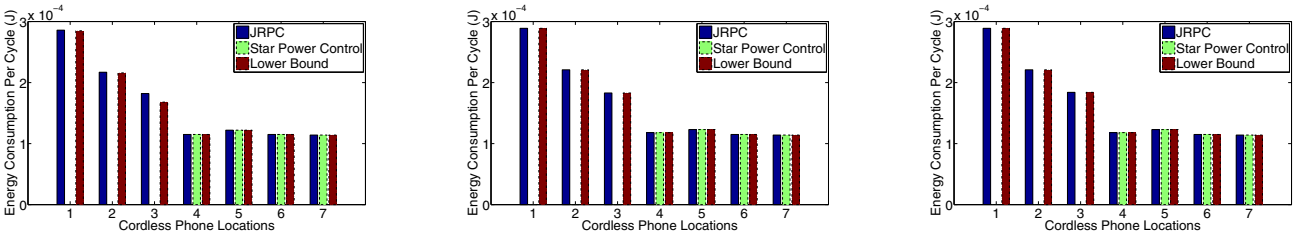

(a) $\lambda_{th} = 0.85$ (b) $\lambda_{th} = 0.95$ (c) $\lambda_{th} = 0.98$

Fig. 7. Power consumption in one cycle in the presence of cordless phone interference

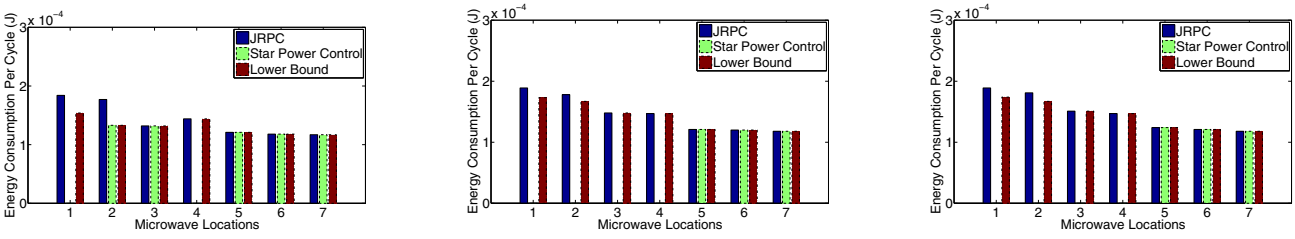

(a) $\lambda_{th} = 0.85$ (b) $\lambda_{th} = 0.95$ (c) $\lambda_{th} = 0.98$

Fig. 8. Power consumption in one cycle in the presence of microwave oven interference

Locations	1	2	3	4	5	6	7
$\lambda = 0.98$	20 ms	20 ms	16 ms	16 ms	14 ms	14 ms	14 ms

TABLE II
END-TO-END DELAY IN THE PRESENCE OF MICROWAVE OVEN CTI AT DIFFERENT LOCATIONS AND WITH DIFFERENT E2E PDR REQUIREMENTS

Location	1	2	3	4	5	6	7
$\lambda = 0.98$	30 ms	22 ms	20 ms	14 ms	14 ms	14 ms	14 ms

TABLE III
END-TO-END DELAY IN THE PRESENCE OF CORDLESS PHONE CTI AT DIFFERENT LOCATIONS AND WITH DIFFERENT E2E PDR REQUIREMENTS

($\lambda_{th} = 0.98$). For the other two thresholds (0.85 and 0.95), the delays are almost the same, thus are not shown here.

C. Protocol Overhead

Our protocol has minimal traffic overhead, as in the link PDR measurement and prediction phase the actual data packets are used instead of probing packets. Active probe packets are only needed for one big slot duration initially to bootstrap the protocol. For the same reason, the time overhead is also minimal as we don't need to allocate additional slots to measure the links' quality. In each big slot, only two extra TDMA cycles are needed separately for the nodes to report their incoming link's PDR estimations to the CU, and for the CU to broadcast the derived power assignments and routing decisions. These control packets are transmitted according to the same power allocation and routing scheme to ensure E2E reliability. In our implementation a big slot contains 40 TDMA cycles, thus the overhead in terms of communication, delay, and energy is merely 5%. Note that, although our current algorithm is centralized, as a BAN has small physical span, it is not an overkill. A distributed algorithm may lead to lower overhead, but will also be less optimal.

VI. Related Work

BAN Performance Measurements Natarajan et al. performed a realistic measurement study [26] for the link layer performance of 2.4GHz BANs. They found that link PDR is highly affected by the environment but less by individuals. However, they did not characterize of the impacts of non-protocol-compliant CTI. Chowdhury et al. [3] measured the impact of microwave ovens and found the link PDR can be greatly reduced; however their study is conducted in a general sensor network but not a BAN. In contrast, we use more external CTI sources, and uncover their heterogenous impact on BAN links and gave explanations.

Power-Controlled Routing Protocols Various power-controlled routing protocols have been proposed in ad hoc and sensor wireless networks, with the objective of minimizing energy to extend network lifetime while maintaining or maximizing/minimizing throughput/delay [1], [2], [10], [23]. Energy-optimal topology-control protocols were also proposed to maintain connectivity [7], [11], [24], [29]. However, those early works all assumed a binary channel propagation model (either 1 or 0 packet reception), which makes the energy optimization problem much simpler than ours. Moreover, none of them considered external CTI; rather, they focused on avoiding the interference among nodes in the same network under traditional physical- or protocol-interference models. In contrast, our model is realistic, i.e., each link is modeled as probabilistic, due to both channel uncertainty and external CTI.

Meanwhile, there are only a few works on power-controlled convergecast [4], [33]. Incel et al. [4] proposed minimum schedule length data collection where power control is used to mitigate the effects of intra-network interference. Ghosh et al. [8] studied the throughput-delay tradeoffs for convergecast using spanning trees. However, not only their goals are different, but also they adopt ideal channel models, which are not applicable to a BAN.

The closest work to ours is [21], an energy-efficient topology control protocol in sensor networks where a probabilistic link model is used. They reduce energy consumption by opportunistically selecting links to form a topology, while maintaining network reachability (theoretically can have multiple paths).

The key difference from ours is, they assumed single transmit power level and do not allow power-control. The Dijkstra algorithm with multiplicative cost metric is also used to find an initial topology, but without considering multiple power levels.

CTI Mitigation Techniques Recent works addressed the mitigation of inter-network interference from protocol compliant networks including both 802.15 (ZigBee) and 802.11 (WiFi) [5], [12], [13], [17], [30], or co-existence between ZigBee and WiFi [15], [38]. However, the type of CTI sources we study are non-protocol-compliant, whose behaviors dramatically differ from 802.x devices. In addition, [3], [15] proposed to exploit the time-domain white space of WiFi for ZigBee performance assurance. However the non-protocol-compliant CTI is persistent and high power - the whitespace either does not exist or is not enough to satisfy the performance goals.

Recently, Gollakota et. al. [9] first studied the cancellation of cross-technology interference for WiFi devices. However, their method requires advanced hardware (multiple antennas). Recently, the feasibility of using power control to defend against constant jamming (similar to some CTI signals) [28], [36] was noticed, but no power-control protocol has been proposed for anti-jamming in multi-hop wireless networks.

VII. Conclusion and Future Work

In this paper, for the first time we study the problem of reliability assurance under external CTI in a BAN, especially those from non-protocol-compliant sources that are much harder to mitigate than the CTI from 802.x devices. We propose a joint routing and power control optimization approach to overcome the impact of such strong CTI in a BAN, while using minimal overall energy consumption. We also exploit passive measurement and prediction to model the uncertain impact of CTI on link qualities. Remarkably, evaluation results show that our JRPC protocol can effectively enlarge the "reliability zone" of the BAN, even when the CTI source is closest to the body. Our protocol also achieves high efficiency, low-energy consumption and overhead. Future work will focus on: 1) Exploring approximation algorithms for optimization. 2) Study the effectiveness of JRPC in more dynamic scenarios.

References

[1] P. Bergamo, A. Giovanardi, R. Giovanardi, A. Travasoni, D. Maniezzo, G. Mazzini, and M. Zorzi. Distributed power control for energy efficient routing in ad hoc networks. *Wireless Networks*, 10:29–42, 2004.

[2] J.-H. Chang and L. Tassiulas. Energy conserving routing in wireless ad-hoc networks. In *IEEE INFOCOM 2000*, volume 1, pages 22 –31 vol.1, 2000.

[3] K. Chowdhury and I. Akyildiz. Interferer classification, channel selection and transmission adaptation for wireless sensor networks. In *Communications, 2009. ICC '09*, pages 1 –5, june 2009.

[4] O. Durmaz Incel, A. Ghosh, B. Krishnamachari, and K. Chintalapudi. Fast data collection in tree-based wireless sensor networks. *Mobile Computing, IEEE Transactions on*, 11(1):86 –99, jan. 2012.

[5] G. Fang, E. Dutkiewicz, K. Yu, R. Vesilo, and Y. Yu. Distributed inter-network interference coordination for wireless body area networks. In *IEEE GLOBECOM 2010*, pages 1 –5, dec. 2010.

[6] A. Gaffney. Fcc releases regulations governing medical body area network devices.

[7] Y. Gao, J. Hou, and H. Nguyen. Topology control for maintaining network connectivity and maximizing network capacity under the physical model. In *IEEE INFOCOM 2008*, pages 1013 –1021, april 2008.

[8] A. Ghosh, O. Incel, V. Kumar, and B. Krishnamachari. Multichannel scheduling and spanning trees: Throughput–delay tradeoff for fast data collection in sensor networks. *Networking, IEEE/ACM Transactions on*, (99):1–1, 2011.

[9] S. Gollakota, F. Adib, D. Katabi, and S. Seshan. Clearing the rf smog: making 802.11n robust to cross-technology interference. In *Proceedings of the ACM SIGCOMM 2011 conference*, SIGCOMM '11, pages 170–181, New York, NY, USA, 2011. ACM.

[10] J. Gomez, A. T. Campbell, M. Naghshineh, and C. Bisdikian. Paro: supporting dynamic power controlled routing in wireless ad hoc networks. *Wirel. Netw.*, 9(5):443–460, Sept. 2003.

[11] M. Hajiaghayi, N. Immorlica, and V. Mirrokni. Power optimization in fault-tolerant topology control algorithms for wireless multi-hop networks. *Networking, IEEE/ACM Transactions on*, 15(6):1345 –1358, dec. 2007.

[12] J. Hauer, V. Handziski, and A. Wolisz. Experimental study of the impact of wlan interference on ieee 802.15. 4 body area networks. *Wireless Sensor Networks*, pages 17–32, 2009.

[13] J. Hou, B. Chang, D. Cho, and M. Gerla. Minimizing 802.11 interference on zigbee medical sensors. In *BodyNets'09*, page 5. ICST, 2009.

[14] J. Huang, S. Liu, G. Xing, H. Zhang, J. Wang, and L. Huang. Accuracy-aware interference modeling and measurement in wireless sensor networks. In *ICDCS '11*, pages 172–181, 2011.

[15] J. Huang, G. Xing, G. Zhou, and R. Zhou. Beyond co-existence: Exploiting wifi white space for zigbee performance assurance. In *ICNP '10*, pages 305–314, 2010.

[16] X. Li, N. Mitton, and D. Simplot-Ryl. Mobility prediction based neighborhood discovery in mobile ad hoc networks. In *IFIP NETWORKING'11*, pages 241–253, 2011.

[17] C. Liang, N. Priyantha, J. Liu, and A. Terzis. Surviving wi-fi interference in low power zigbee networks. In *ACM SenSys*, pages 309–322. ACM, 2010.

[18] X. Liang, X. Li, Q. Shen, R. Lu, X. Lin, X. Shen, and W. Zhang. Exploiting Prediction to Enable Secure and Reliable Routing in Wireless Body Area Networks. In *INFOCOM*, Orlando, FL, 2012.

[19] S. Lin, G. Zhou, K. Whitehouse, Y. Wu, J. A. Stankovic, and T. He. Towards stable network performance in wireless sensor networks. In *RTSS '09*, pages 227–237, 2009.

[20] S. Liu, G. Xing, H. Zhang, J. Wang, J. Huang, M. Sha, and L. Huang. Passive interference measurement in wireless sensor networks. In *IEEE ICNP*, pages 52 –61, oct. 2010.

[21] Y. Liu, Q. Zhang, and L. Ni. Opportunity-based topology control in wireless sensor networks. *IEEE TPDS*, 21(3):405 –416, march 2010.

[22] K. Lorincz, D. Malan, T. Fulford-Jones, A. Nawoj, A. Clavel, V. Shnayder, G. Mainland, M. Welsh, and S. Moulton. Sensor networks for emergency response: challenges and opportunities. *IEEE Pervasive Computing*, 3(4):16–23, Oct.-Dec. 2004.

[23] J. Luo, C. Rosenberg, and A. Girard. Engineering wireless mesh networks: Joint scheduling, routing, power control, and rate adaptation. *Networking, IEEE/ACM Transactions on*, 18(5):1387 –1400, oct. 2010.

[24] R. Madan, S. Cui, S. Lall, and A. Goldsmith. Cross-layer design for lifetime maximization in interference-limited wireless sensor networks. In *IEEE INFOCOM 2005*, volume 3, pages 1964–1975. IEEE, 2005.

[25] H. Madsen. *Time Series Analysis: Forecasting and Control*, volume 77. CRC Press, 2008.

[26] A. Natarajan, B. de Silva, K.-K. Yap, and M. Motani. Link layer behavior of body area networks at 2.4 ghz. In *Proceedings of the 15th annual international conference on Mobile computing and networking*, MobiCom '09, pages 241–252, New York, NY, USA, 2009. ACM.

[27] M. Patel and J. Wang. Applications, challenges, and prospective in emerging body area networking technologies. *Wireless Communications, IEEE*, 17(1):80 –88, february 2010.

[28] K. Pelechrinis, I. Broustis, S. V. Krishnamurthy, and C. Gkantsidis. Ares: an anti-jamming reinforcement system for 802.11 networks. In *CoNEXT '09*, pages 181–192, 2009.

[29] R. Ramanathan and R. Rosales-Hain. Topology control of multihop wireless networks using transmit power adjustment. In *IEEE INFOCOM 2000*, volume 2, pages 404 –413 vol.2, 2000.

[30] R. Shah and L. Nachman. Interference detection and mitigation in ieee 802.15. 4 networks. In *IEEE IPSN*, pages 553–554, 2008.

[31] Shimmer. Wireless strain gauge.

[32] D. Smith, L. Hanlen, J. Zhang, D. Miniutti, D. Rodda, and B. Gilbert. Characterization of the dynamic narrowband on-body to off-body area channel. In *IEEE ICC'09*, pages 1–6. IEEE, 2009.

[33] S. Upadhyayula, V. Annamalai, and S. Gupta. A low-latency and energy-efficient algorithm for convergecast in wireless sensor networks. In *Global Telecommunications Conference, 2003. GLOBECOM'03. IEEE*, volume 6, pages 3525–3530. IEEE, 2003.

[34] Q. Wang, M. Hempstead, and W. Yang. A realistic power consumption model for wireless sensor network devices. In *IEEE SECON '06*, volume 1, pages 286 –295, sept. 2006.

[35] S. Xiao, A. Dhamdhere, V. Sivaraman, and A. Burdett. Transmission power control in body area sensor networks for healthcare monitoring. *IEEE JSAC*, 27(1):37 –48, january 2009.

[36] W. Xu. On adjusting power to defend wireless networks from jamming. In *MOBIQUITOUS '07*, pages 1–6, Washington, DC, USA, 2007. IEEE Computer Society.

[37] K. Y. Yazdandoost and K. Sayrafian-Pour. Ieee p802. 15 wireless personal area networks - channel model for body area network (ban). *IEEE P802.15-08-0780-06-0006, IEEE P802.15 WG for WPANs*, Apr. 2009.

[38] X. Zhang and K. Shin. Enabling coexistence of heterogeneous wireless systems: Case for zigbee and wifi. In *Proc. of ACM MobiHoc*, 2011.

[39] J. Zhu. On the power efficiency and optimal transmission range of wireless sensor nodes. In *IEEE EIT'09*, pages 277 –281, june 2009.